4
Growth of Nanocrystals in Solution

R. Viswanatha and D. D. Sarma

4.1
Introduction

Tunability of various physical and chemical properties of materials by varying the size in the region of nanometers has opened up many new directions in several fields of current research and modern technologies [1, 2]. In particular, the study of systematic changes in the electronic structure of solids as a function of size in this nanometric regime has been intensively investigated in recent times (see for example Refs. [3–6]). Sustained efforts in this field have established interesting applications such as UV protection films [7], fluorescent sensors in biological applications [8], photocurrent generation in various devices [9], optical switches [10], catalytic reactions [11], nanotweezers [12] and other optoelectronic devices [13]. One of the major aspects necessary for the actual realization of these applications is the ability to synthesize nanocrystals of the required size with a controlled size distribution. The growing demand to obtain such nanocrystals is met largely by the solution route synthesis of nanocrystals [14, 15], due to its ease of implementation and high degree of flexibility. The main difficulty with this method is that the dependences of the average size and the size distribution of the generated particles on parameters of the reaction are not understood in detail and, therefore, the optimal reaction conditions are arrived at essentially in an empirical and intuitive manner [16]. The understanding of coarsening processes that lead to growth of the minority phase within a majority phase by combining smaller particles is important both scientifically and for technological considerations [17–21]. In recent times, there has been a renewed interest in understanding the growth process of a solid phase within another solid in the nanometric regime. Interestingly, the kinetics of the growth of a solid from a solution, which is the most popular chemical method to produce a wide variety of systems with dimensions in the nanometer region, has been relatively less investigated [22–26]. However, there is a popular belief that the growth in solution occurs via a diffusion limited Ostwald ripening process [14, 15].

Nanomaterials Chemistry. Edited by C. N. R. Rao, A. Müller, and A. K. Cheetham

ISBN: 978-3-527-31664-9

In this chapter, we briefly discuss the theory of nucleation. We then review the various theoretical aspects of the different processes that influence the growth rate. Following the discussion of the theoretical framework, we review experimental progress made in investigating the growth of various nanocrystals.

4.2 Theoretical Aspects

The growth of nanocrystals in solution involves two important processes, the nucleation followed by the growth of the nanocrystals. We discuss these two processes in the following two subsections.

4.2.1 Theory of Nucleation

La Mer and coworkers [27] studied extensively nucleation and growth in sulfur sols, from which they developed an understanding of the mechanism for the formation of colloids or nanocrystals from a homogeneous, supersaturated medium. Their mechanism suggested that a synthesis of the colloid should be designed in such a way that the concentration increases rapidly, rising above the saturation concentration for a brief period, when a short burst of nucleation occurs with the formation of a large number of nuclei in a short space of time. These particles grow rapidly and lower the concentration below the nucleation level whilst allowing the particles to grow further at a rate determined by the slowest step in the growth process, thus separating the nucleation and growth in time. La Mer's mechanism is depicted schematically by means of the simple diagram shown in Fig. 4.1. The requirements for monodispersity, as evident from La Mer's diagram, are a high rate of nucleation leading to the burst of nuclei formation in a short period, an initial fast rate of growth of these nuclei to reduce the concentration below the nucleation concentration rapidly and an eventual slow rate of growth leading to a long growth period compared to the nucleation period. They also derived the rates of growth of sols prepared by the above-mentioned dilution method. The growth rates obtained were reproduced from previous theoretical considerations which allowed the estimation of the value of the diffusion coefficient of sulfur. It was also claimed that the application of this method to the estimation of diffusion coefficients was valid for any colloidal system that was characterized by a small particle size distribution at all stages of its growth. Further, a qualitative explanation was offered for the necessary conditions under which mono-dispersed colloids might be prepared by both the dilution and acid decomposition of sodium thiosulfate methods. This mechanism of La Mer was later widely applied in attempts to prepare various nearly-monodisperse particles in homogeneous solutions [28], yet success was achieved only after tedious trial-and-error attempts to tune the major parameters such as the concentration of reactants. So far it has not been possible to have a generalized approach to the

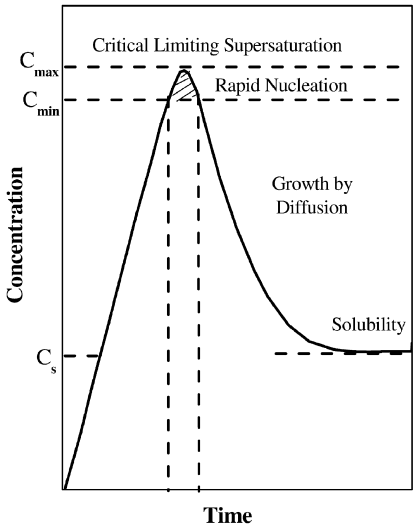

Fig. 4.1 Schematic diagram illustrating La Mer's condition for nucleation.

synthesis of different systems by following the necessary conditions of La Mer [29]. Generalizations between preparations have been few and it is now believed that La Mer's mechanism is rigorously appropriate only for the system for which it was developed, that is sulfur sols, and it may not have significance as a general approach to a wide variety of systems. It was later observed that La Mer's condition for nucleation is neither a necessary nor sufficient condition for monodispersity but that the specific growth mechanism also plays an important role in deciding the size and the size distribution.

Regardless of the rigorous validity of La Mer's prediction in the context of diverse systems, the key idea of separating the nucleation stage and growth process in time is often used to obtain nearly monodisperse particles. In most of the cases in recent times, synthesis has been carried out by mixing the reactants together, often by injecting one of the components into the remaining ones, in a very short time. This is to ensure that the entire nucleation takes place in that short time, followed by a much slower growth process, thereby attempting to separate the two stages temporally. In the next subsection, we discuss the various aspects of the mechanism of the growth of nanocrystals from solution.

4.2.2 Mechanism of Growth

Nucleation occurs over some time with constant monomer concentration. Eventually surface growth of clusters begins to occur which depletes the monomer supply. When the monomer concentration falls below the critical level for nucleation (critical supersaturation level), nucleation ends. A general analysis of the growth

process is then important to understand nanocrystal synthesis. In general, the surface to volume ratio in smaller particles is quite high. As a result of the large surface area present, it is observed that surface excess energy becomes more important in very small particles, constituting a non-negligible percentage of the total energy. Hence, for a solution that is initially not in thermodynamic equilibrium, a mechanism that allows the formation of larger particles at the cost of smaller particles reduces the surface energy and hence plays a key role in the growth of nanocrystals. A colloidal particle grows by a sequence of monomer diffusion towards the surface followed by reaction of the monomers at the surface of the nanocrystal. Coarsening effects, controlled either by mass transport or diffusion, are often termed the Ostwald ripening process. This diffusion limited Ostwald ripening process is the most predominant growth mechanism and was first quantified by Lifshitz and Slyozov [30], followed by a related work by Wagner [31], known as the LSW theory.

The diffusion process is dominated by the surface energy of the nanoparticle. The interfacial energy is the energy associated with an interface due to differences between the chemical potential of atoms in an interfacial region and atoms in neighboring bulk phases. For a solid species present at a solid/liquid interface, the chemical potential of a particle increases with decreasing particle size, the equilibrium solute concentration for a small particle is much higher than for a large particle, as described by the Gibbs–Thompson equation. The resulting concentration gradients lead to transport of the solute from the small particles to the larger particles. The equilibrium concentration of the nanocrystal in the liquid phase is dependent on the local curvature of the solid phase. Differences in the local equilibrium concentrations, due to variations in curvature, set up concentration gradients and provide the driving force for the growth of larger particles at the expense of smaller particles [32].

Now, assume that the average radius of the particles is r. The bulk liquid phase is considered to have a uniform supersaturated monomer concentration, c_b, while the monomer concentration at the particle interface, c_i and the solubility of the particle with a radius r is given by c_r. The flux of monomers, J, passing through a spherical surface with radius x within the diffusion layer, is given by Fick's first law as

$$J = 4\pi x^2 D \, \mathrm{d}C/dx \tag{4.1}$$

At steady state, where J is constant over the diffusion layer x, the above equation can be integrated approximately to obtain

$$J = \frac{4\pi D r(r+\delta)}{\delta}(c_b - c_i) \tag{4.2}$$

where, δ is the thickness of the diffusion layer.

This flux can be equated to the consumption rate of the monomer species at the surface of the particle. That is,

$$J = 4\pi r^2 k_d (c_i - c_r) \tag{4.3}$$

where k_d is the rate constant of a simple first order deposition reaction. In solution, it is difficult to measure c_i and hence it is necessary to eliminate that variable from the two equations. Assuming that $dr/dt = JV_m/4\pi r^2$, we get

$$\frac{dr}{dt} = \frac{\frac{D}{r}\left(1 + \frac{r}{\delta}\right) V_m (c_b - c_r)}{1 + \frac{D}{k_d r\left(1 + \frac{r}{\delta}\right)}} \tag{4.4}$$

The terms c_b and c_r are related to the particle radius, r, by the Gibbs–Thompson equation given by the expression

$$c_r = c_\infty \exp\left(\frac{2\sigma V_m}{rRT}\right) \approx c_\infty \left(1 + \frac{2\sigma V_m}{rRT}\right) \tag{4.5}$$

where c_∞ is the concentration of a flat particle, σ is the interfacial energy, V_m is the molar volume and R is the universal gas constant. The approximate expression on the right is derived by retaining only the first two terms in the expansion of the exponential function under the assumption of a small value of the argument, $2\sigma V_m/rRT$.

Similarly, c_b can be written as

$$c_b = c_\infty \exp\left(\frac{2\sigma V_m}{r_b RT}\right) \approx c_\infty \left(1 + \frac{2\sigma V_m}{r_b RT}\right) \tag{4.6}$$

Since diffusion layer thicknesses are typically of the order of microns, in the case of nanocrystals we assume that $r \ll \delta$. Substituting Eqs. (4.5) and (4.6) into Eq. (4.4) we obtain the equation

$$\frac{dr}{dt} = \frac{2\sigma V_m^2 c_\infty}{RT(1/D + 1/k_d r)} \frac{(1/r_b - 1/r)}{r} \tag{4.7}$$

We shall now explore the different behaviors of growth arising from this differential equation in various limits.

4.2.2.1 Diffusion Limited Growth: Lifshitz–Slyozov–Wagner (LSW) Theory and Post-LSW Theory

Diffusion limited growth: When the diffusion is the slowest step in the growth process, characterized by $D \ll k_d r$ in Eq. (4.7), the particle growth is essentially controlled by the diffusion of the monomers to the surface. In this limit, Eq. (4.7) reduces to the form,

$$\frac{dr}{dt} = \frac{2\sigma D V_m^2 c_\infty}{RT} \frac{(r/r_b - 1)}{r^2} = K_D(r/r_b - 1)/r^2 \tag{4.8}$$

where K_D, given by $2\sigma D V_m^2 c_\infty / RT$, is a constant. If the total mass of the system is explicitly kept conserved, the LSW theory showed that the ratio r/r_b is a constant. Making this assumption in Eq. (4.8), we see that Eq. (4.8) reduces to the form

$$\frac{dr}{dt} = K_D{}^* \text{const}/r^2 \tag{4.9}$$

that can be easily solved to obtain the dependence of the particle size on time. It is given by

$$r^3 - r_0^3 = Kt \tag{4.10}$$

where r_0 is the average radius of the particle at time $t = 0$. K is given by the expression

$$K = \frac{8\sigma D V_m^2 c_\infty}{9RT} \tag{4.11}$$

where D, the diffusion constant of the system at any given temperature, is given by the equation, $D = D_0 \exp(-E_a/k_b T)$.

LSW theory: The original idea of a growth mechanism driven by the reduction of the surface energy was proposed by Ostwald in 1901 [33]. It is interesting to note that a quantitative theory based on these ideas was derived [30, 31] nearly 50 years after Ostwald's discovery of the phenomenon. The discovery of the LSW theory marked one of the major advances in the theory of Ostwald ripening. The LSW theory, considering a diffusion limited growth, but following a different and more rigorous method than that described earlier, was able to make quantitative predictions on the long-time behavior of the coarsening process.

The LSW approach is based on the following basic assumptions.

- This theory examines the growth of spherical particles in a supersaturated medium.
- Particles are assumed to grow or shrink only in relation to the mean field concentration set at infinity.
- The total mass of the solute is conserved.
- The size distribution of the growing phase under the assumption of being spherical is characterized only by a radius distribution in terms of a continuous function, valid in the limit of a sufficiently large number of particles in the system to justify such a continuum description.
- Processes such as nucleation and aggregation that introduce new particles are negligible.

Using these assumptions, they arrived at a universal asymptotic solution. First, the concept of a critical radius, r_b, was introduced, which separated the smaller sized particles ($r < r_b$), shrinking in size, from the larger particles ($r > r_b$) that became larger with time. When the radius r is found to be equal to r_b, the growth is found to be zero. In the asymptotic limit, it was shown that the ratio of the mean radius, r, of the system of particles to the critical radius, r_b, is a constant.

It is interesting to note that the asymptotic state of the system is predicted to be independent of the initial conditions. This was obtained as a direct consequence of the mass conservation of the solute on the asymptotic solution of the continuity equation and the kinetic equation. These authors further showed that the time evolution of distribution of radii of the particles at any given time has the following functional form,

$$D(\xi) = \kappa\xi^2 \left(\frac{3}{3+\xi}\right)^{7/3} \left(\frac{1.5}{1.5-\xi}\right)^{11/3} \exp\left(\frac{-\xi}{1.5-\xi}\right) \tag{4.12}$$

where, $\xi = x/r$, x is the radius of various particles and r the average mean radius and κ depends only on time t by the relation $\kappa = \kappa_c/(1 + t/\tau_D)^{4/3}$. τ_D is the time constant given by the expression

$$\tau_D = \frac{9r_0^3 RT}{64\sigma D C_\infty V_m^2} \tag{4.13}$$

We have illustrated a typical form of the distribution function, $D(\xi)$, in Fig. 4.2. This functional form shows a typical characteristic asymmetry at the higher particle diameter side cutting off sharply when the radius is 1.5 times the average radius. Further, integrating Eq. (4.12), they obtained an expression for the average radius, r, of the particle at time t, given by $r^3 - r_0^3 = Kt$, similar to Eq. (4.10).

Post-LSW theories: The coarsening phenomenon has been experimentally investigated in diverse systems, including detailed studies involving precipitate for-

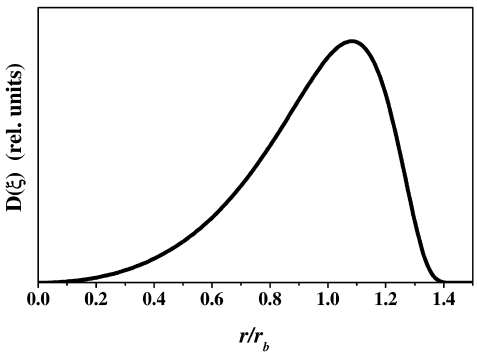

Fig. 4.2 Typical line shape of the size distribution of a purely diffusion-controlled reaction as predicted by the LSW theory.

mation in alloys, like Co in Cu–Co alloy [34] and Ni in Ni–Fe alloys [35]. It was observed that while the temporal power law for r, (i.e., $r^3 \propto t$) was confirmed by these experiments [36], the temporal evolution of the size distribution did not agree with that of the experimental results. The experiments, in general, showed a broader and more symmetric distribution. Further experiments also showed that there exists a dependence of the rate constant K on the volume fraction [37], where the volume fraction is defined as the ratio of the volume of the particular phase to that of the total volume of the system. While the LSW theory is a pioneering work in this field, it does not consider the effects of the finite volume fraction of the coarsening phase. We now take a look at the post-LSW theories, taking into account the finite volume fraction of the growing phase. Moreover, the LSW theory assumes that their rate equation is valid at a very low volume fraction, ϕ, of the coarsening phase, such that the coarsening rate is independent of the surroundings. This unspecified low volume fraction, being much lower than realistic values of ϕ encountered in typical experiments, led to disagreements between experimental results and theoretical predictions. These disagreements were found to be due the high strength of the diffusional interactions between neighboring particles that arose from the long-range coulomb interaction surrounding the particles. This can be taken into account by statistically averaging the diffusional interactions of the particle with its surroundings.

In order to improve the theoretical description beyond the LSW description, several groups addressed theoretically some of the above-mentioned shortcomings of the original theory. The prominent ones among them include the works by Brailsford and Wynblatt [38], Voorhees and Glickman [39], Marqusee and Ross [40] and Tokuyama and Kawasaki [41]. It is surprising to note that each of the groups have used identical microscopic equations to perform the statistical averaging of the growth rate and arrive at qualitatively different results; this apparently intriguing situation arises from using different methods of averaging, such as chemical rate theory, computer simulation techniques, a multiple scattering method or a scaling expansion technique. However, all these theories agree on some of the points. For example, the temporal power law reported in the LSW theory is not dependent on the volume fraction, ϕ, validating this aspect of LSW theory. On the other hand, the particle size distribution function becomes broader and more symmetric than the LSW distribution with an increase in the volume fraction. The rate constant, K, rises rapidly at low volume fractions and is followed by a slower increase at higher volume fractions. The predictions of the different theoretical works mentioned above are almost identical till a volume fraction of 0.1, unlike the predictions of LSW theory that did not show any dependence of the rate constant K on the volume fraction. However, these theories do not agree with each other on several other important aspects. For example, the dependence of the rate constant K on the volume fraction ϕ was predicted to follow $K(\phi) - K(0) \sim \phi^{(1/2)}$ in Ref. [40] but $K(\phi) - K(0) \sim \phi^{(1/3)}$ in Ref. [39].

The above discussion shows that while the LSW theory represented a considerable advance in describing the diffusion-controlled Ostwald ripening quantitatively, it is an oversimplified approach in many respects in comparison to the

complex and diverse situations encountered in actual practice. Though later works made significant progress by accounting for some of the concerns arising from the drastic assumptions in the LSW theory, these still left unanswered a large number of questions about the size distribution in the diffusion-controlled growth. For example, it is not known what particle size distribution results from nucleation followed by the growth process and if this influences the system's approach to the asymptotic state. Moreover, at $\phi \neq 0$, diffusional interactions between particles are present and thus the spatial distribution of the particles becomes important. However, all the theories described earlier assume random spatial distribution of particles and the role of spatial correlations between particles is largely ignored; it is not yet fully understood how these assumptions may affect the description of the growth kinetics.

4.2.2.2 Reaction-limited Growth

So far, we have only considered the diffusion-limited regime, characterized by $D \ll k_d r$ in Eq. (4.7). Besides the diffusion process, that is accounted for in the LSW theory, another important process in the growth of any particle is the reaction at the surface where the units of diffusing particles are assimilated into the growing nanocrystal. We now turn to this opposite limit of reaction-limited growth.

If $k_d r \ll D$ in Eq. (4.7), then the growth rate is limited by the surface reaction of the monomers. Then the rate law for the average radius of growing nanocrystals can be reduced from Eq. (4.7) to the form given by

$$\frac{dr}{dt} = \frac{2\sigma k_d V_m^2 c_\infty}{RT} \frac{(r/r_b - 1)}{r} = K_R(r/r_b - 1)/r \tag{4.14}$$

If the conservation of mass is valid, similar to the diffusion limited case, the ratio of the average radius to the critical radius (r/r_b) is observed to be constant [32, 66]. Hence the above differential equation in the case of simple first order reaction can be integrated under this assumption to give rise to the equation of the form

$$r^2 \approx K_R t \tag{4.15}$$

Thus, it can be seen that the mean particle size grows as a function of the square root of time. The size distribution in the case of the reaction controlled Ostwald ripening was established long back by Wagner [31] and is expected to follow the equation of the form

$$D(\xi) = \kappa_R \xi \left(\frac{2}{2-\xi}\right)^5 \exp\left(\frac{-3\xi}{2-\xi}\right) \tag{4.16}$$

where, $\xi = x/r$ and κ_R depends on time t by the relation $k_R = k'/(1 + t/\tau_R)^2$. τ_R is the time constant given by the expression

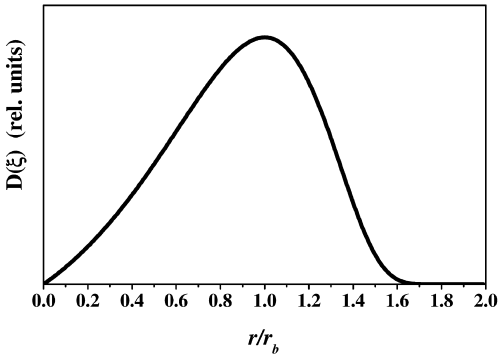

Fig. 4.3 Typical line shape of the size distribution of a purely reaction-controlled reaction as predicted by Wagner.

$$\tau_R = \frac{r_{b0}^2 RT}{\sigma k_d C_\infty V_m^2} \tag{4.17}$$

The typical form of the distribution function in the case of reaction controlled kinetics is shown in Fig. 4.3. The above expression is valid for radii less than two times the critical radius r_b after which the distribution goes to zero. In contrast, in the diffusion limited case, the distribution function was found to go to zero at 1.5 times the critical radius. It is observed that the size distribution in the reaction limited growth is broader and more symmetrical than that obtained from the diffusion-controlled growth (Fig. 4.2 and Eq. (4.12)).

4.2.2.3 Mixed Diffusion–Reaction Control

While in the preceding two sections, we have discussed the two limiting cases, in practice it is to be expected that both diffusion and surface reaction will contribute to the growth process in real experimental conditions, rendering the applicability of the limiting cases uncertain and of doubtful relevance in general. Specifically, several recent reports [42, 44, 66] have stressed that the growth in a variety of realistic systems does not belong to either of the two limits, namely the diffusion- or the reaction-limited regimes, but is controlled by a combination of diffusion and reaction at the surface.

It has been shown by LSW theory that, when the mass is conserved, the ratio r/r_b is a constant and equal to one in the diffusion-limited case [30]. Later, it was observed that, in the reaction-limited case, when the mass is kept conserved, r/r_b is a constant and equal to 8/9 [45]. Recently it was shown [42, 66] that if the conditions in limiting cases can be extended to the intermediate case, in other words if r/r_b is assumed to be a constant, K', Eq. (4.7) takes the form

$$\frac{dr}{dt} = \frac{2K'\sigma V_m^2 c_\infty}{RTr_2(1/D + 1/k_d r)} \tag{4.18}$$

This equation can be simplified and written in the following form

$$\frac{r^2\,\mathrm{d}r}{D^*\mathrm{const}} + \frac{r\,\mathrm{d}r}{k_\mathrm{d}{}^*\mathrm{const}} = \mathrm{d}t \tag{4.19}$$

which can be easily integrated to obtain

$$t = Ar^3 + Br^2 + C \tag{4.20}$$

where $A = RT/2DK'\sigma V_\mathrm{m}^2 c_\infty$ and $B = RT/2k_\mathrm{d}K'V_\mathrm{m}^2 c_\infty$ and C is a constant. Thus, this expression, while separating the diffusion and the reaction terms, provides us with an analytical solution for the transient growth regime under the assumptions mentioned above. These expressions were found to explain satisfactorily some of the experimental observations [66] discussed in a later section.

Talapin et al. [44] have further suggested that the growth of nanocrystals could not be satisfactorily explained by approximating the Gibbs–Thompson equation (Eqs. (4.5) and (4.6)) to just the first two terms of the exponential expansion. We note that the size of the growing crystal, r, appears in the denominator of the argument for the exponential function in Eq. (4.5). This implies that the argument becomes increasingly larger for decreasing r, thereby making the finite polynomial expansion of the exponential function increasingly inaccurate. Thus, it is necessary to go beyond such an approximate expression, as used earlier (see Eq. (4.5)), particularly in the case of nanocrystal growth. Hence retaining the exponential term in the Gibbs–Thompson equation and assuming $r \ll \delta$ in Eq. (4.4) they obtain the equation

$$\frac{\mathrm{d}r^*}{\mathrm{d}t} = \frac{S - \exp(1/r^*)}{r^* + K\exp[\alpha/r^*]} \tag{4.21}$$

where r^* is the dimensionless average radius given by

$$r^* = \frac{RT}{2\sigma V_\mathrm{m}} r \tag{4.22}$$

The other parameters include the rate constant, K, monomer oversaturation parameter, S, and the dimensionless time τ. They are given by the equations,

$$\tau = \frac{R^2T^2Dc_\infty}{4\sigma^2 V_m} t \tag{4.23}$$

$$K = \frac{RT}{2\sigma V_\mathrm{m}} \frac{D}{k_\mathrm{d}} \tag{4.24}$$

$$S = c_\mathrm{b}/c_\infty \tag{4.25}$$

In arriving at the above equations, the volume fractions were kept lower than 10^{-3}, so that the corrections due to the diffusional interactions between neighbor-

ing particles were not necessary. Monte-Carlo simulations were performed by calculating the remaining monomer concentration and the monomer oversaturation S in each cycle and substituting in Eq. (4.21) to calculate the growth of the next step. Different statistical parameters like oversaturation of monomers, nanocrystal concentration, average particle size, standard deviation in the size distribution were monitored at each step. These calculations included the nucleation step in the growth dynamics and assumed that the nucleation and growth processes were completely separated in time. Though detailed kinetics of nucleation is not known experimentally in real systems, these calculations suggested that the influence of initial conditions on the growth of nanocrystals was negligibly small as long as the rate of nucleation was much higher than the growth rate. This part of the result is in agreement with that of the LSW theory predicting a unique shape of the particle size distribution independent of the initial conditions of nucleation. In the case of the growth of a single nanocrystal, some amount of the monomer is consumed in the reaction. For growths with a finite volume of solution, the bulk concentration of monomer and the value of the oversaturation S decrease gradually. This gives rise to a shift in the critical radius towards larger sizes and the growth rate decreases.

In the case of nanocrystal ensembles with a diffusion-controlled growth, this approach predicts that an initially symmetric normal radius distribution, as well as the standard deviation, evolves in time toward the asymmetric negatively signed one. Initial conditions have significant influence on the size distribution only in a short transient period and only minor changes were observable at later stages of growth. When the reaction at the surface is much slower than the diffusion process, thereby becoming the rate determining step, the particle size distribution is found to be systematically broader than observed for diffusion-controlled growth. In the diffusion-controlled growth, in the early period, it is observed that the growth rate is much higher than predicted by the LSW theory. The narrowest size distribution is achieved when the particle growth is influenced more by the diffusion process than the reaction at the surface. They also established conditions for the evolution of ensembles leading to either ''focusing'' or ''defocusing'' of the particle size distribution. It was observed that the size distribution of the nanocrystal in the early stages of growth underwent a strong focussing effect if the particles had high initial oversaturation parameters, in other words, a large excess of the monomers. The excess of monomer affects strongly the evolution of the size distribution during the initial stages of nanocrystal growth. A fast increase in r accompanied by a strong narrowing in the size distribution is observed, followed by subsequent broadening without almost any change in r. However, the value of r and the standard deviation depend on the initial monomer concentration. The nanocrystals have initially positive growth rates and smaller nanocrystals grow faster than the larger ones. The number of particles remains nearly constant during the stage of ''focusing'' of the size distribution. During the focusing stage the size distribution remains nearly symmetric, and it is well described by a normal distribution. The defocusing is accompanied by a transition from symmetric to asymmetric stationary size distribution. During

the focusing stage the oversaturation drops to some equilibrium value, and the number of nanocrystals starts to decrease due to the dissolution of the smallest particles.

4.3 Experimental Investigations

Having discussed the theoretical framework, we now review in this section the experimental situation in investigating the growth kinetics of various nanocrystals. Though the potential of solution phase synthesis of metals and metal oxide nanocrystals has long been realized, there were few mechanistic studies on these systems till about a decade ago. However, in this past decade, there has been a surge of interest [14, 15, 46–55, 66] in understanding the growth mechanism in nanocrystals. As already mentioned, the growth of nanocrystals is believed to take place predominantly via diffusion-limited coarsening, known as ''Ostwald ripening''. This has been reported so far for the cases of TiO_2 [46], InAs and CdSe [14] and ZnO [47] nanocrystal growth. Typically in any such experiment, the average size of the growing nanocrystal is monitored by measuring for example, the average diameter, d, of spherical particles as a function of the time, t and then analyzing whether d^3 is proportional to t in accordance with the prediction of the LSW theory (see Eq. (4.10)). The average size of nanocrystals can be measured either directly employing microscopic techniques or indirectly by monitoring a size-dependent physical property, for example absorption or emission energies and then deducing the size from the measured quantity with the use of a suitable calibration curve that relates the physical property to the size of the nanocrystals. For example, Oskam et al. [46] studied the growth kinetics of TiO_2 by transmission electron micrograph (TEM) recorded at various stages of growth, arriving at the conclusion that the growth can be described by the $d^3 \propto t$ prediction of the LSW theory.

Though TEM is the most direct tool to analyze the size and the size distribution in nanocrystals, it is a very time consuming process and it would be impossible to follow the size and size distribution of a fast growing particle during the synthesis by this technique. Moreover, *in situ* monitoring of the growth of nanocrystals in a solution is obviously beyond the scope of TEM. Therefore alternative methods have been devised and employed in recent times to probe *in situ* growth of nanocrystals in real time. Since the scattering of electromagnetic waves is a pronounced function of the particle size, this phenomenon is being used increasingly to study *in situ* growth of various nanocrystal systems. Considering the nanometer size of these particles in the region of interest, small angle X-ray scattering (SAXS), particularly using synchrotron radiation, becomes a powerful tool to probe the growth of nanocrystals in the size regime of typically 0.5–10 nm with a sub-second time resolution [54, 56].

Viswanatha et al. [54] used time-resolved SAXS at a third-generation synchrotron source to study the growth of CdS nanocrystals in the absence of any cap-

ping agents. They studied the dependence of the average diameter of growing nanocrystals and found it to follow the cube-root of time dependence, indicative of an Ostwald ripening mechanism. Further, it was established that the growth kinetics rigorously follows the LSW theory, not only in terms of the growth of the average diameter of the nanocrystals, but also in terms of the time dependence of the size distribution and the temperature dependence of the rate constant, establishing a remarkable adherence to the diffusion-limited growth or Ostwald ripening in the quantum confinement (<5 nm) regime.

Another alternate approach, based on the optical properties of nanocrystals, has also gained recent popularity as an effective tool to investigate the growth mechanism. It is well-known that the bandgap of nanocrystals in the small sized (<10 nm) regime is generally a strongly varying function of the size; this phenomenon is often termed the quantum size effect. It has been extensively probed both experimentally and theoretically. Based on a range of theoretical approaches to calculate the electronic structure of nanocrystals, such as *ab initio* methods [57], semi-empirical pseudo-potential methods [58, 59], and parametrized tight binding methods [60–67], it is now possible to quantitatively estimate the size of the semiconducting nanocrystal from the shift in bandgap obtained from UV absorption data. This has led to an extensive increase in the study of growth kinetics in recent times by monitoring the time-dependent UV absorption of *in situ* reaction mixtures. Recently, it has been shown that it is also possible to estimate the size distribution from UV absorption data [53] and also photoluminescence data [14]. This has led to a considerable advance in the study of growth kinetics in semiconductor nanocrystals.

Peng et al. [14] used UV absorption to determine the size of the nanocrystals and the width of the photoluminescence data to determine the size distribution to study the growth of CdSe and InAs nanocrystals. They observed a focusing and defocusing effect similar to that expected of Ostwald ripening behavior. More recently, Qu et al. [68] developed an *in situ* method of measuring the UV absorption of solutions at high temperatures and carried out real time measurements with a time resolution of a few milliseconds. They showed that in the case of CdSe the growth consists of a prolonged formation of relatively small particles (nucleation) followed by a focusing of the size distribution when the distribution changed from an asymmetric line shape to a symmetric one. This stage was followed by a stable phase which is most likely due to the monomer concentration in the solution being close to the solubility of the particles in the solution. The fourth stage showed the relatively large particles in the distribution growing even bigger while the relatively small ones in the solution disappeared. Hence the authors suggested this stage as the main course of the Ostwald ripening process.

Metal nanocrystals, like Au and Ag are known to show intense plasmon bands in the visible region, which can be easily monitored by optical absorption spectroscopy. Recently, it has been shown by Scaffardi et al. [69] that the size of the nanocrystal can be obtained from Mie theory [70] by analyzing the width of the plasmon band in the case of smaller particles (<10 nm) and by analyzing the po-

sition of the band for larger particles. This observation suggests the possibility of studying the growth of the metal nanocrystals by monitoring the time evolution of the spectral features of the plasmon band during the chemical reaction leading to the growth of metal nanocrystals.

In the following sections, we critically review typical growth kinetics with illustrative examples from the literature. Recently it was shown that an apparently linear dependence of d^3 on t, especially only in the asymptotic limit, does not rigorously establish the validity of the LSW theory, although this criterion has been used [46, 47] extensively in earlier studies of growth of such particles. In general, d^x as a function of t may appear linear within the experimental error limit for a wide range of x-values. Therefore, it becomes necessary to verify explicitly the expected dependences of the rate constant on temperature and the concentrations of the reactants, which provide more sensitive and critical testing grounds for the growth mechanism. More detailed studies on these systems suggest that, in most cases, the growth kinetics cannot be explained within the framework of diffusion-limited Ostwald ripening. We discuss in detail one example of the growth of metal nanocrystals, using Au as a test case [72], and one example of semiconducting nanocrystals, using ZnO [48, 53, 55, 66] as an illustration; these studies show that the growth kinetics often violates the over-simplified predictions of a simple diffusion-limited growth model, in contrast to the popularly held belief of the validity of diffusion-limited Ostwald ripening of nanocrystals in such cases.

4.3.1 Au Nanocrystals

Interest in the colloidal metal particles dates back to the time of Michael Faraday who recognized that the different colors of gold sols could be indicative of the different sizes or states of aggregation of the particles. An aspect of importance in the context of metal particles is the phenomenon of nucleation and growth in the nanometer regime. As early as 1951, a similar study was carried out by Turkevich et al. [71] on colloidal gold kinetics of gold sols in the micron length scales. In recent times Seshadri et al. [72] have studied the growth kinetics of gold in the nanometric regime quite extensively using transmission electron microscopy; we discuss this work in detail here to illustrate the complex growth mechanism of metallic nanocrystals. They studied the growth kinetics by investigating the particle size distribution at various times. It was observed that the growth was initially quick, slowing down at longer times. A plot of the mean diameter as a function of $t^{1/3}$ was found to be nearly a straight line, as expected in the case of Ostwald ripening. However, in contrast to the prediction of LSW theory in the context of the diffusion-limited Ostwald ripening process, the size distribution was nearly symmetric and it was found that it could be described well by a Gaussian profile, as shown in Fig. 4.4. While LSW and other theories of growth predict an asymmetric size distribution function (see Eqs. (4.12) and (4.16) and Figs. 4.2 and 4.3), attempts to use asymmetric profiles were not successful in describing the experimental results. It is possible to arrive at a more symmetric size distribution

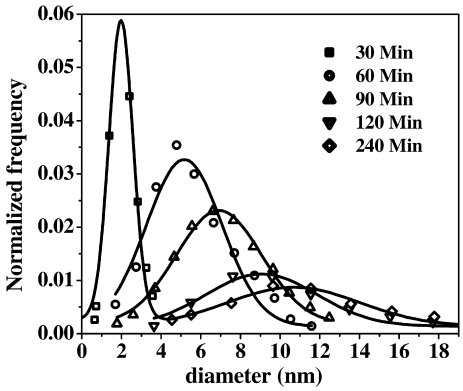

Fig. 4.4 Typical variation of the particle size distribution at various time intervals. The solid lines show the Gaussian fits to the experimental data. (Adapted from Ref. [72].)

within the LSW theory, but this happens only at high enough volume fractions. Considering that the volume fractions in these specific studies were below 10^{-4}, an exceptionally high volume fraction cannot be invoked to explain the experimentally observed symmetric size distribution. This report suggests that the growth process should be essentially stochastic and implies that the nucleation and growth is well separated. Further, it is observed that the average diameter and the standard deviation show the same time dependence. Normalized intensity as a function of x/r collapses into a single curve, thereby suggesting that it is a stochastic process. It was concluded that the growth was activated, since the growth kinetics showed a temperature dependence. This report provides a new growth law to fit the observed particle size distribution and its time dependence. However, further investigation is required to understand the growth mechanism completely in such cases.

4.3.2 ZnO Nanocrystals

Growth kinetics in the case of ZnO nanocrystals is one of the earliest [47] as well as the most extensively investigated systems [48–50, 52, 53, 55, 66, 73]. However, the study of the growth kinetics of ZnO nanocrystals from solutions has been fraught with contradictory claims till recently. It has been known for a long time that ZnO can be synthesized using zinc acetate ($Zn(OAc)_2$) and a base such as NaOH. However, the intriguing aspect in the preparation of the samples has been the observation that the presence of a small or even trace amount of water in the synthesis of ZnO nanocrystals influences strongly the size of the nanocrystals [74, 75]. In order to understand the extraordinary sensitivity of ZnO nanocrystal size to the presence of any trace amount of water, we first review the growth kinetics of ZnO in the absence of any base and only in the presence of

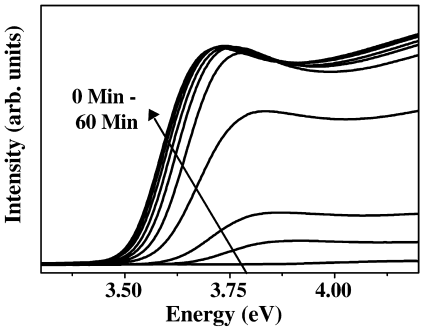

Fig. 4.5 UV absorption curves obtained at equal intervals of time for a typical reaction carried out at 318 K with 100 mM of water. (Adapted from Ref. [66].)

precisely defined quantities of water. One of the first reports of the growth kinetics of ZnO using water as a reactant was put forth recently by Hu et al. [55]. They studied the growth kinetics of ZnO by measuring the time-resolved UV absorption spectra and by analyzing the shift in the band edge using the effective mass approximation (EMA) [76]. However, it has long been shown that EMA overestimates the size of the nanocrystal and hence is not a very reliable tool to obtain the size of nanocrystals. Here we discuss the work carried out more recently in our own group, circumventing the earlier shortcomings [66].

A typical set of optical absorption spectra for a given concentration of reactants and at a fixed temperature (Fig. 4.5) shows a clear increase in the absorption intensity with increasing time. This suggests an increase in ZnO concentration with time. More significantly, there is a systematic shift in the absorption edge to lower energies with increasing time, indicating a steady growth of larger particles. The average diameter, d, of the nanocrystals was estimated from the dependence of the bandgap on particle size, based on a realistic tight binding modeling of first principle electronic structure calculations for ZnO [66], which is known to provide a realistic variation in the bandgap energy with size, unlike the earlier proposed EMA. We show typical variations of the cube of the diameter, d, vs. the time, t for several temperatures in Fig. 4.6(a). Since the size information from the shift in the absorption edge is derived indirectly via the dependence of the electronic structure on the size of the nanocrystals, the sizes obtained from the analysis of the absorption spectra were verified at a few specific points in time by monitoring the TEM intermittently.

Though the d^3 vs. t behavior deviates from the expected linearity based on the LSW theory (see Eq. (4.10)) in the small time regime, it indeed follows a linear relation at higher time-scales remarkably well, shown by thick solid lines, as if suggesting a dominantly diffusion-limited growth in the long time limit. However, it has also been noted that these results show acceptable linear behavior within experimental uncertainties for x-values ranging from 2.3 to 4, as illus-

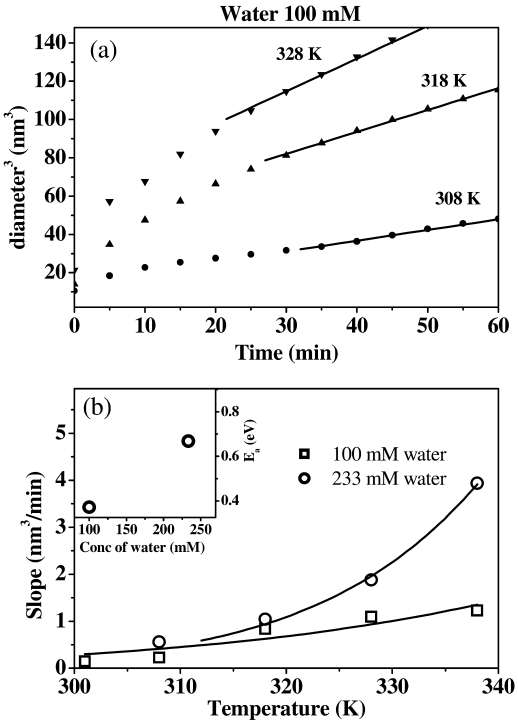

Fig. 4.6 (a) Variation of the cube of diameter of ZnO nanocrystals shown as a function of time for different temperatures at a fixed water concentration (233 mM). (b) The variation of the slopes of the linear part as a function of temperature for different water concentrations. The solid lines show the fits obtained from the function of the form given in Eq. (4.11). The inset shows the variation of the activation energies as a function of concentration of water. (Adapted from Ref. [66].)

trated by a plot of d^4 vs. t for the same set of $d(t)$ used for Fig. 4.7, indicating the difficulty in establishing the mechanism of growth kinetics only on the basis of the value of the exponent in $d^x \propto t$ plots. In order to probe the growth mechanism more rigorously, it is necessary to go beyond the simple verification of the d^3 vs. t plot being linear or not. It should be noted here that the slope (K) of the linear plot of d^3 vs. t has a well-defined dependence on the temperature, T, via the dependence of the diffusion constant, D, on T (see Eq. (4.11)). One can easily obtain the slopes, K, from the linear plots in Fig. 4.6(a) at different temperatures for various concentrations of the reactants, namely water in this case. Least-squared error fits of the K value to the form described in Eq. (4.11) show that though the observed dependence of K on T is reasonably well described by this functional form at higher concentration of water, the fit is far from satisfactory for lower water concentration, as shown in Fig. 4.6(b). Even more significantly, the activation energy, E_a, obtained from the best-fit curves and plotted

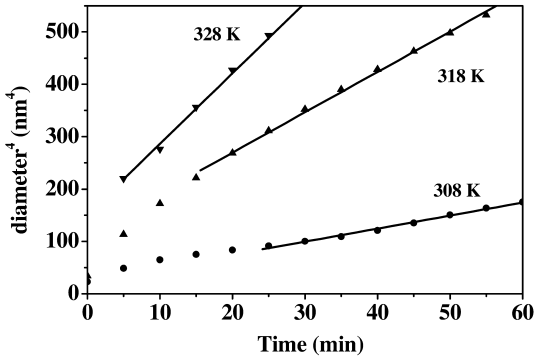

Fig. 4.7 Variation of the fourth power of the diameter of ZnO nanocrystals shown as a function of time for different temperatures at a fixed water concentration (233 mM).

(open circles) in the inset of Fig. 4.6(b) clearly shows a pronounced dependence on the concentration of water. This is clearly an unphysical situation, since the activation energy associated with the diffusion is clearly a function of the solvent and cannot depend on the solute concentration in the dilute limit (typically < 10 mmol of the reactant). This clearly suggests that a purely diffusion-controlled mechanism cannot explain the observed growth laws, in spite of the apparently linear behavior of the d^3 vs. t plots.

In the case of the present reaction of zinc acetate with water to form ZnO nanocrystals, the Zn^{2+} ions are obtained by the complete dissociation of zinc acetate into Zn^{2+} and OAc^- ions. The hydroxyl ions for the reaction are obtained from the dissociation of water. Ideally the nanocrystals of ZnO are assumed to comprise tetrahedrally coordinated Zn and O atoms and only the surface Zn atoms are terminated with a hydroxyl ion instead of the O ion. Small ZnO clusters are nucleated at time $t = 0$. The growth of the clusters occurs by the dehydration of terminating OH^- ion using the freely available dissociated OH^- ion in the solution. It is followed by the capturing of the Zn^{2+} ions available in the solution and brought near the surface of the cluster by the process of diffusion. The growth of the nanocrystal is thus further continued by the Zn^{2+} ion capturing the OH^- ion and so on. Hence the Zn^{2+} ions and the OH^- ions in solution may be considered as the pseudo-monomers of the growth process. In this present model the availability of the OH^- ions is governed by the dissociation of water. This is, however, controlled by the dissociation constant of water and hence the reaction cannot be assumed to be instantaneous. The presence of a prolonged reaction suggests that there should be an increase in the concentration of ZnO nanocrystals, at least for the lower concentrations of water. Further, it should be noted that the dissociation constant of water increases by a couple of orders of magnitude with increasing temperature providing a large number of OH^- ions at higher temperatures and thus increasing the rate of the

reaction drastically. Thus the reaction mechanism to form ZnO can be written as $H_2O \leftrightarrow H^+ + OH^-$, $Zn^{2+} + 2OH^- \leftrightarrow Zn(OH)_2 \leftrightarrow ZnO + H_2O$.

A colloidal particle grows by a sequence of monomer diffusion towards the surface due to the concentration gradients set up by the differences in local curvatures and then the reaction of the monomers on the surface. Since the absorbance in the UV absorption spectrum increases with time (Fig. 4.5), it is clear that the reaction forming ZnO take place over time scales comparable to that of the growth of the nanocrystals, especially at lower temperatures and lower concentrations of water, suggesting that the nucleation is not separated from the growth. The reaction mechanism suggests that both the diffusion of Zn^{2+} ions and the rate at which the reactions take place at the surface have to be taken into consideration in the modeling of the growth process. Clearly then the growth in these nanocrystals belong to the transient regime of growth, discussed in the earlier section. Analyzing the reaction mechanism, using Eq. (4.7), it can be seen that the reaction term is relatively more important for small d, which is consistent with our observation (Fig. 4.6(a)) of more marked deviations from a purely diffusion-controlled growth at early times or the initial stages of the growth, when the nanocrystals are evidently the smallest in size. Replacing average radius r by the average diameter d in Eq. (4.20), we obtain the relation, $t = Bd^3 + Cd^2 +$ const, with $B = KT \exp(E_a/k_B T)$ and $K \propto 1/(D_0 \gamma V_m^2 c_\infty)$. The coefficient C is of the form $C \propto T/k_d \gamma V_m^2 c_\infty$. Using this expression relating d and t in the transient regime of growth, the experimentally observed variation $d(t)$ can be fitted for different temperatures, as shown in Fig. 4.8 by thick solid lines through experimental data obtained at different temperatures. The remarkable goodness of fits over

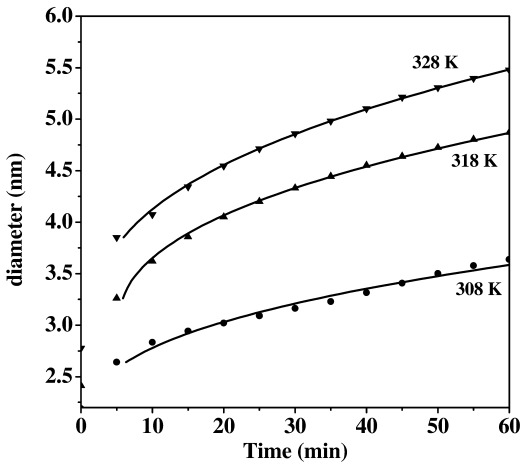

Fig. 4.8 Variation of the diameter of ZnO nanocrystals shown as a function of time for different temperatures at a fixed water concentration (100 mM). (Adapted from Ref. [66].)

the entire time regime, in contrast to those in Fig. 4.6(a), provides a conclusive validation of this description for the growth of ZnO nanocrystals. Further, the values of B for different temperatures and different concentrations of water can be extracted from the fits. The expected temperature dependence of the coefficient B was carried out and the activation energy, E_a, obtained from the least square fits to $B(T)$, can be plotted as a function of water concentration. While the results for the activation energy obtained earlier assuming only a diffusion-controlled growth (shown in the inset of Fig. 4.6(b)) exhibited a pronounced dependence on the water concentration, the new estimates of E_a using the transient growth model recovers a physically acceptable scenario of concentration-independent activation energy, 0.74 ± 0.01 eV. This firmly establishes the proposed growth mechanism.

We note here that the linear dependence of d^3 on t has often been used in the past literature to conclude about the growth model in a wide variety of systems, such as TiO_2 [46], CdSe [14], and ZnO [55]. However, in view of the results discussed here, it is clear that the cubic dependence of diameter on time alone is not enough to determine the mechanism of growth for nanocrystals and it is necessary to study the other dependences. One such example of growth studies was performed in the group of Searson to study the growth of ZnO in the presence of a base such as NaOH. The distinguishing feature of this case compared to the previous example is that a strong base (NaOH) providing a very large number of OH^- ions is used to carry out the reaction in contrast to the presence of only water, providing OH^- concentration of the order of 10^{-7}. We note here that most of the syntheses of ZnO nanocrystals, independent of the growth studies, indeed use such a base to carry out the reaction to form ZnO [47, 80].

The growth kinetics in the presence of a base, such as NaOH, as the reactant has been extensively studied by Searson et al. [47, 49, 51, 55]. They have measured the *in situ* UV absorption spectra for the reaction carried out at different temperatures. The bandgap thus obtained is converted to the size of the particle using EMA. They have shown that the cube of the diameter of the particles is linearly dependent on the time, as expected by the LSW theory. Further, they have obtained the values of σ and V_m from literature and determine c_∞ experimentally. Using these values, they have calculated the value of the diffusion coefficient D from the slopes of the linear curves. For the case of ionic diffusion, it is known that the diffusion constant can be obtained by the Stokes–Einstein relation given by

$$D = k_B T / 6\pi\eta a \tag{4.26}$$

where η is the viscosity of the solvent and a is the hydrodynamic radius of the solute. The values obtained for the diffusion coefficient from the value of the slope K were compared with that of the Stokes–Einstein diffusion model and found to be consistent with the typical values for ions in solution at room temperature and in good agreement with that obtained from the Stokes–Einstein model.

These authors have also studied the effects of various anions like $Zn(OAc)_2$, $ZnBr_2$ and $Zn(ClO_4)_2$ on the growth kinetics. They found that that the particle growth at longer time is determined solely by diffusion in the case of $Zn(OAc)_2$ and $ZnBr_2$. However, in the case of $Zn(ClO_4)_2$, the radius increases more rapidly than for coarsening. The authors suggested that aggregation could be a competing mechanism of growth to the coarsening process and is dependent on surface chemistry resulting in either oriented or random attachment of particles. Random aggregation usually leads to the formation of porous clusters of particles whereas epitaxial attachment of particles leads to the formation of secondary particles with complex shapes and unique morphologies. They believe that the faster increase in the radius in the case of $Zn(ClO_4)_2$ arises due to epitaxial aggregations, resulting in much larger particles. The rate constants were obtained for all three different anions and plotted in the Arrhenius plot. From this plot, the activation energies were calculated to be 0.21 eV for $ZnBr_2$, 0.35 eV for $Zn(OAc)_2$ and 0.46 eV for $Zn(ClO_4)_2$. They also studied the effect of solvents on the kinetics by using ethanol, propanol, butanol, pentanol and hexanol as solvents in separate reactions. It is found that the coarsening rate constant increases not only with increasing temperature, but also with longer solvent chain length. The effect of solvent chain length on the rate constant is believed to arise from solvent viscosity, surface energy, and the bulk solubility of ZnO in these different solvents. These results illustrate that the solvent is an important parameter in controlling details of the growth kinetics.

A very recent work [53] has suggested a non-monotonic dependence of growth on the NaOH concentration, thus indicating a qualitative departure from the Ostwald ripening behavior. This suggests that the growth mechanism in ZnO is quite complex; while it has been extensively studied, more experiments are needed to understand completely the growth mechanism in these nanocrystals.

4.3.3
Effect of Capping Agents on Growth Kinetics

So far, we have discussed the growth of nanocrystals in the absence of any capping agent, which, when present, inhibits the growth of nanocrystals by effectively passivating their surfaces. However, the synthesis of almost all nanocrystals is in reality carried out in the presence of a capping agent to stabilize the desired size for a given application, thereby making the growth process complex and beyond the scope of LSW theory. The effect of the capping agent on the modification of the growth kinetics is very specific to the choice of capping agent, thereby defying any general theoretical approach; additionally very little is known about the growth process in such a complex reaction. In particular, there is hardly any theoretical approach to understanding such non-ideal reaction conditions. On the other hand, it is obvious that a detailed understanding of such growth processes is essential, if we are to employ rational syntheses rather than empirical ones. Thus, there have been a few attempts to probe experimentally different growth processes in the presence of a variety of passivating agents in order to understand

the influence that each reaction parameter has on the average size and the size distribution. We present here a few selected examples of technologically important systems, like CdSe and ZnO, to illustrate some of the important points.

4.3.3.1 Effect of Oleic Acid on the Growth of CdSe Nanocrystals

CdSe nanocrystals have attracted the attention of many groups because of the possibility of tuning their emission wavelength through the entire visible spectrum by changing their size and the high quantum efficiency of such emission. Peng et al. [14] discovered a very facile reaction for the synthesis of high quality CdSe nanocrystals. However, a capping agent is inherently present in the synthesis, making it necessary to study the role of capping agents in such a reaction. This was recently discussed in detail by Bullen et al. [78] for the case of oleic acid and TOP as capping agents. As the nuclei grow, van der Waals interactions can cause rapid coalescence of nuclei and an unrestrained particle growth. However, capping agents may be added during the synthesis to adsorb and limit particle–particle aggregation, though such molecules may, in principle, also hinder monomer deposition. For example, ligands such as oleate and TOP are chemically bonded to both the precursor and the particles that form and hence hinder particle growth.

Bullen et al. carried out time-resolved UV absorption and fluorescence measurements. From the shift in the absorption edge due to quantum confinement effects, they obtained the sizes of the nanocrystals using the bandgap shift vs. size calibration data presented by Yu et al. [79]. The nucleation of CdSe in hot octadecene can provide an ideal environment for instantaneous nucleation, using up all the monomers; therefore, a subsequent reduction in the temperature allows only the growth of the particle, thus providing an ideal system to separate out nucleation and particle growth in solution. The number of nuclei formed during the nanocrystal synthesis and an estimation of the initial size of these nuclei prior to growth have been studied [78]. It was found that the nuclei concentrations were constant throughout the reaction, within experimental error, and that it is a very fast process that ceases almost immediately after monomer injection. It was observed that the rate is controlled by the reaction at the surface and a rate equation was obtained. It was found that the rate of growth of the nanocrystal is influenced by two effects. The surface area of each nanocrystal increases over time tending to make the reaction rate accelerate; on the other hand, decreasing concentrations of Cd and Se monomers cause the growth rate to slow down. As a consequence of these two opposite trends, the radius is observed to grow almost linearly at very early times. However, the growth rate proceeds toward saturation in the long time regime. These results can be understood in the following way using the chemical rate equation. The rate must obey an equation of the form

$$\frac{\mathrm{d}[\mathrm{Cd}]_t}{\mathrm{d}t} = -kA(t)[\mathrm{Cd}]_t N(t) \tag{4.27}$$

where $[\mathrm{Cd}]_t$ is the concentration of available Cd at time t, $A(t)$ is the surface area

of each particle at time t, $N(t)$ is the number of particles at time t, and k is an interfacial rate constant that reflects the rate determining steps during deposition. Under steady-state growth conditions both Se and Cd should deposit at equal rates, so the particle growth can be described in terms of either species. From the experiments it is observed that the number of particles remains constant following nucleation, i.e., $N(t) = N_0$; furthermore, assuming spherical symmetry we get $A(t) = 4\pi r^2(t)$. Then the rate of increase in the volume of precipitated CdSe in the entire solution is given by

$$\frac{dV}{dt} = -V_m \frac{d[Cd]_t}{dt} \tag{4.28}$$

where V_m is the molar volume of CdSe. From Eqs. (4.27) and (4.28), it is seen that

$$\frac{dr}{dt} = kV_m N_0 [Cd]_t = k[V_m([Cd]_0 - [Cd]_{eq}) - 4N_0\pi r^3/3] \tag{4.29}$$

since the effective concentration of free Cd, $[Cd]_t$, is equal to the initial concentration injected $[Cd]_0$, less the amount already deposited, $[Cd]_{dep} = 4N_0\pi r^3/3V_m$, less the amount remaining at equilibrium, $[Cd]_{eq}$.

At the maximum value of r, given by $r_{max} = (Y/Z)^{1/3}$ where $Y = V_m([Cd]_0 - [Cd]_{eq})$ and $Z = 4N_0\pi/3$, all the excess Cd in solution would have been consumed and hence, the radius was found to saturate after some time. On fitting the data, it was found that the best fits for the rate constant were at least 8 orders of magnitude below the diffusion-limited rate constant. This suggests that the growth occurs at a far slower rate and hence smaller particles are formed. The rate constant for growth did not change significantly with different amounts of capping agents. These results indicated that the oleic acid is not only an efficacious capping agent for CdSe nanocrystals in octadecene, but it markedly influences the primary nucleation steps in two distinct ways. First, the number of nuclei is reduced drastically as oleic acid is added since the nucleation is more difficult in the presence of oleic acid due to its complexation with Cd; the results also show that the initial nuclei in the presence of oleic acid are smaller than in its absence. Secondly, the complexing agent not only reduces the rate of nucleation by reducing the active monomer concentration, but it also rapidly caps the nuclei as they form. These two effects compete with each other. If there is too much capping agent, nucleation can be completely hindered, ultimately leading to indiscriminate growth of a small population of nuclei. However, because there are fewer nuclei formed in the presence of the ligand, larger clusters were unexpectedly found to form with increasing concentration of oleic acid. It is also noted that since the two processes, nucleation and particle growth, are decoupled in this system, there are two, well-defined activation energies. This shows clearly that the capping agents not only determine the rate of growth, but also play a major role in determining the number and size of the nuclei formed during injection; this, in turn, has a very pronounced influence on the subsequent growth rate.

4.3.3.2 PVP as a Capping Agent in the Growth of ZnO Nanocrystals

Various reports in the literature [66, 80] have now established that polyvinyl pyrollidone (PVP) is an effective capping agent to restrict the growth of ZnO nanocrystals. The temporal evolution of the average diameter, d, as a function of time, t, for the different ratios of Zn^{2+} to PVP is shown for a fixed NaOH concentrations in Fig. 4.9 [53]. The figure shows that there is a rapid and sustained growth of nanocrystals with time in every case, in spite of the presence of the capping agent. It was found that it was not possible to fit any of the curves to the form $d^x - d_0^x = Kt$, for any given value of x, even for the case without any PVP. This suggests that the growth process observed here is qualitatively different from the Ostwald ripening mechanism, even in the absence of any capping agent, as discussed in a previous section. The present example, involving the presence of a capping agent [53] is even less understood and is certainly beyond the scope of the LSW theory. In the absence of any guidelines provided by a theoretical understanding, it was noted that an empirical fit in terms of $(d - d_0)^x = Kt$ describes well the experimental results in every case, as shown by the best fit results with the solid lines overlapping the experimental data points in Fig. 4.9.

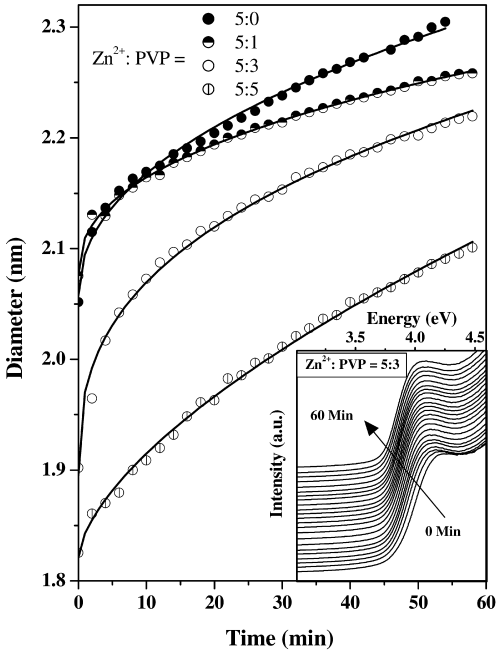

Fig. 4.9 Variation in the size of ZnO nanocrystals shown as a function of time for different ratios of Zn^{2+} to PVP at a fixed concentration (0.5 mmol) of NaOH. The inset shows the UV absorption curves for a typical system as a function of time ranging from 0 to 60 min. (Adapted from Ref. [53].)

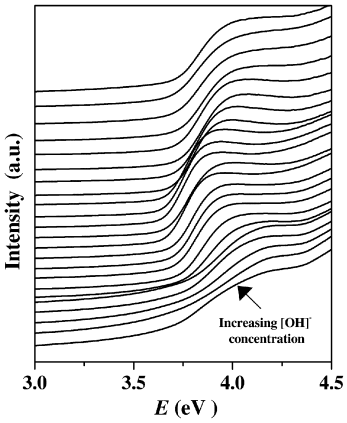

Fig. 4.10 The UV absorption curves recorded for ZnO nanocrystals with Zn^{2+} to PVP ratio of 5:3 as a function of NaOH concentration varying from 0.04 to 1 mmol at fixed time of 160 min after the addition of NaOH. (Adapted from Ref. [53].)

Further, it was observed that the absorption edge of the products after a fixed time of reaction appears at different energies for different concentrations of NaOH, as shown in Fig. 4.10. It is observed to vary non-monotonically, thereby indicating the complex dependence of the average nanocrystal size on NaOH concentration. Additionally, the sharpness of the absorption edge is found to vary significantly and non-monotonically as a function of NaOH concentration. These intriguing non-monotonic dependences of the size and size distribution on NaOH concentration after a fixed reaction time are shown in Fig. 4.11. Fig. 4.11(a) shows the expected result that the average particle size is largest in the absence of PVP (Zn^{2+} to PVP ratio = 5:0). A low Zn^{2+} to PVP ratio of 5:1 is also found to be inefficient in passivating the nanocrystals (Fig. 4.11(b)), minimal changes were observed compared to the uncapped system (Fig. 4.11(a)) in terms of both size and size distribution. However, the average size of the nanocrystal was found to decrease systematically as the PVP concentration was increased, as shown in Fig. 4.11(c) and (d). The results shown in Fig. 4.11 reveal that the dependences of d on the concentration of NaOH for all concentrations of PVP were essentially similar.

The insets to Fig. 4.11(a) and (b) revealed a slight monotonic increase in the relative distribution at low PVP concentration as the NaOH concentration increases. Interestingly, at higher concentrations of PVP (insets to Fig. 4.11(c) and (d)), we observed a striking decrease in the size distribution or a ''narrowing'' effect. This narrowing effect was understood in the following way. In the presence of high concentrations of PVP and the absence or low concentration of NaOH, the ZnO-like clusters are formed using the oxide ions from the PVP and isopropanol in the medium catalyzed by the slight basicity of the medium. In this case the rate determining step of the reaction is found to be the formation of the ZnO-like clusters and these clusters are immediately capped efficiently with PVP. Therefore, further ripening that leads to more uniform sized clusters is strongly suppressed at higher PVP concentration due to the effective passivation. This is also suggested by the fact that there is hardly any growth of the nanocrystal size

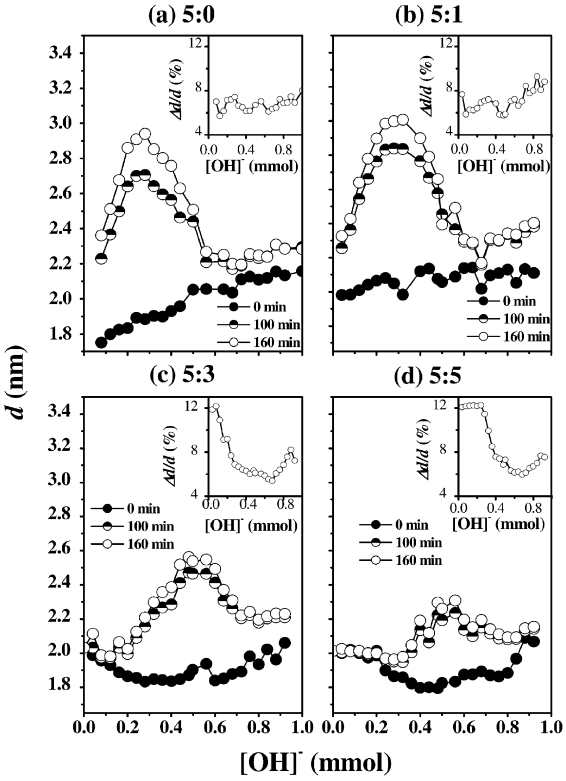

Fig. 4.11 Variation in the size of ZnO nanocrystals plotted as a function of NaOH concentration at times 0 min (closed circles), 100 min (half-open circles), and 160 min (open circles) for Zn^{2+} to PVP ratios of (a) 5:0, (b) 5:1, (c) 5:3, and (d) 5:5. The corresponding insets show the variation in size distribution at 160 min. (Adapted from Ref. [53].)

with time, indicated by the overlap of the three time (0, 100 and 160 min) plots, for the large PVP concentrations (Fig. 4.11(c) and (d)) in the low NaOH concentration regime. Hence, a broad size distribution was observed in such cases. Beyond a certain critical concentration of NaOH, namely about 0.1 to 0.2 mmol in Fig. 4.11(c) and (d) respectively, an evident growth of the nanocrystal size with time was observed, suggesting that, at these higher concentrations, NaOH is effective in reacting with the small pre-formed ZnO clusters in spite of the presence of PVP, thereby leading to the growth, though at a much slower rate than in the uncapped case. This removal of the capping agent at higher concentration of NaOH also allows a ripening process in competition with the passivating process by PVP, that gives rise to a higher degree of uniformity in size. Interestingly it was also noted that the minimum in the relative deviation corresponds to the same NaOH concentration that is required to just reach the low size regime in the range of the higher NaOH concentration regime. If the NaOH concentration

is higher than this optimal value, the relative deviation becomes larger, leading to a poorer quality of the product, though the average particle size remains approximately the same. Thus, the present study establishes the necessity to use the optimal NaOH concentration to obtain small nanocrystals with a minimum size distribution.

4.3.3.3 Effect of Adsorption of Thiols on ZnO Growth Kinetics

Though the effect of thiols in capping the sulfides is well-known [81], it has been recently observed that the growth of ZnO nanocrystals can be altered by the addition of thiols. Pesika et al. [50] carried out reactions to form ZnO using zinc acetate and a base such as NaOH and studied the effect of the addition of thiol on the growth of ZnO. This was done by adding different amounts of octanethiol to a reaction of ZnO and carrying out an *in situ* UV absorption study. From the observed shifts in the band edge, they obtained the sizes of the nanocrystals using EMA and found that the growth of the nanocrystals is retarded by the addition of octanethiol. Further, it was observed that the retardation is more efficient on increasing the concentration of octanethiol.

We have studied the effect of adding a large amount of thiol on the growth of ZnO nanocrystals, when the capping agent was added after different intervals of time; the results are shown in Fig. 4.12 as plots of *d vs. t*. The vertical error bars on each data point represent the size distribution, while the average size is denoted by the data point itself. The data with filled circles show that the uncapped ZnO continues to grow with time, with the average diameter of the nanocrystals reaching up to ca. 5.5 nm after nearly 2 h. The size distribution also exhibits a

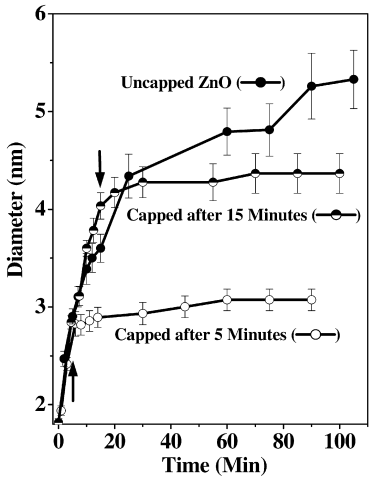

Fig. 4.12 Temporal evolution of the diameter of ZnO nanocrystals with thiol added at different intervals of time. The size distribution is shown as error bars in the graph.

monotonic increase in the uncapped case. The arrows on the other two sets of data mark the time when the thiol was added to the solution. It is interesting to note that with the addition of thiol, the growth continues for a short period of approximately 5 min and then the growth effectively stops. Additionally, the size distribution also does not change with time after a short time of adding the capping agent, as shown by the error bars in Fig. 4.12. Thus, it can be observed that thiol is a very efficient capping agent for ZnO.

The above examples make it clear that though the capping agents are expected to reduce the size and the size distribution, it is necessary to maintain the synthesis condition at the optimal level in order to prevent reversal of roles in the reaction. The study of the growth kinetics in the more realistic and complex cases of capped nanocrystals provide us with a handle to understand the details of growth under actual synthetic conditions and thereby help us to achieve the optimal conditions.

4.4 Concluding Remarks

Solution chemistry is the most versatile and highly flexible technique to tune the size and size distribution of nanocrystals. From a fundamental point of view, the growth kinetics of a solid in solution constitutes a very important field of study; however, there are relatively few such investigations reported in the literature. We have presented in this chapter the growth of nanocrystals from solutions in terms of some of the available theoretical models, followed by specific experimental results as illustrative examples of different growth models. We also indicate how such studies may open up new routes to the rational synthesis of nanocrystals.

It is observed that the growth of nanocrystals can be controlled either by diffusion or by the reaction at the surface. In the diffusion-controlled regime, we have discussed the assumptions as well as the results obtained from the LSW theory. We have also discussed models with specific improvements over the LSW theory in the diffusion-limited regime. We have presented the dependence of diameter and the form of the size distribution in the reaction-limited regime. Then these two limiting behaviors were integrated into a single model which accounts for the regime where both diffusion and reaction at the surface are important. We discussed the essential results obtained within this transient regime at the end of the section dealing with various theoretical models.

While there are several studies in the literature reporting diffusion-limited Ostwald ripening as the mechanism of growth, we present the cases of Au nanocrystals and ZnO nanocrystals, exhibiting remarkable departure from the expected Ostwald ripening process. In the case of Au nanocrystals, it is observed that though the diameter is found to increase as the cube-root of time, the size distributions are found to be very symmetric, unlike that expected for Ostwald ripening behavior. In the case of ZnO nanocrystals synthesized even in the absence of a base, it was found that though $d^3 \propto t$ is satisfied in the asymptotic limit, the

activation energy is found to depend on the concentration of the reactant, if the experimental data are analyzed in the usual manner within the diffusion-limited ripening process. A better analysis suggests that ZnO growth kinetics belong to the transient Ostwald ripening regime.

We have then explored the effects of capping agents on the growth kinetics in three typical cases, namely the effect of oleic acid on the growth of CdSe nanocrystals, PVP on the growth of ZnO and thiol on the growth of ZnO. In all the cases, the capping agent is found to have multiple roles and affects the kinetics in a complicated and unique manner that is beyond the scope of the existing theories.

References

1 *Nanometer Scale Science and Technology*, M. Allegrini, N. Garci, O. Marti (Eds.), IOS Press, Amsterdam, 2001.
2 *Nanotechnology Research Directions: IWGN Workshop report*, M. C. Roco, B. S. Williams, A. P. Alivisatos (Eds.), Kluwer Academic Publishers, Dordrecht, 1999.
3 A. D. Yoffe, *Adv. Phys.* **50**, 1 (2001).
4 A. P. Alivisatos, *J. Phys. Chem.* **100**, 13226 (1996).
5 *Encyclopedia of Nanoscience and Nanotechnology*, H. S. Nalwa (Ed.), American Scientific Publishers, 2004.
6 *Chemistry of Materials*, C. N. R. Rao, A. K. Cheetham, A. Muller (Eds.), Wiley-VCH, Weinheim, 2004.
7 E. A. Meulenkamp, *J. Phys. Chem. B*, **102**, 5566 (1998).
8 M. Bruchez Jr., M. Moronne, P. Gin, S. Weiss, A. P. Alivisatos, *Science*, **281**, 2013 (1998).
9 J. Nanda, K. S. Nagaraj, B. A. Kuruvilla, G. L. Murthy, D. D. Sarma, *Appl. Phys. Lett.*, **72**, 1335–1337 (1998).
10 C. T. Tsai, D. S. Chuu, G. L. Chen, S. L. Yang, *J. Appl. Phys.*, **79**, 9105–9109 (1996).
11 A. T. Bell, *Science*, **299**, 1688 (2003).
12 P. Boggild, T. M. Hansen, C. Tanasa, F. Grey, *Nanotechnology*, **12**, 331 (2001).
13 H. Lin, S. Tzeng, P. Hsiau, W. Tsai, *Nanostruct. Mater.*, **10**, 465–477 (1998).
14 X. Peng, J. Wickham, A. P. Alivisatos, *J. Am. Chem. Soc.*, **120**, 5343 (1998).
15 W. W. Yu, X. Peng, *Angew. Chem. Int. Ed.*, **41**, 2368 (2002).
16 J. S. Bradley, in *Clusters and Colloids. From Theory to Applications*, G. Schmid (Ed.), VCH, New York, 1994.
17 A. Onuki, *Phase Transition Dynamics*, Cambridge University Press, Cambridge, 2002.
18 A. J. Bray, *Adv. Phys.*, **43**, 357 (1994).
19 K. Binder, P. Fratzl, in *Phase Transformations in Materials*, G. Kostorz (Ed.), Wiley-VCH, Weinheim, 2001.
20 G. R. Carlow, M. Zinke-Allmang, *Phys. Rev Lett.*, **78**, 4601 (1997).
21 J. Alkemper, V. A. Snyder, N. Akaiwa, P. W. Voorhees, *Phys. Rev. Lett.*, **82**, 2725 (1999).
22 C. A. Jeffrey, E. H. Conrad, R. Feng, M. Hupalo, C. Kim, P. J. Ryan, P. F. Miceli, M. C. Tringides, *Phys. Rev. Lett.*, **96**, 106105 (2006).
23 P. Gangophadhyay, R. Kesavamoorthy, S. Bera, P. Magudapathy, K. G. M. Nair, B. K. Panigrahi, S. V. Narasimhan, *Phys. Rev. Lett.*, **94**, 047403 (2005).
24 S. Takakusagu, K. Fukui, R. Tero, F. Nariyuki, Y. Iwasawa, *Phys. Rev. Lett.*, **91**, 066102 (2003).
25 A. F. Craievich, G. Kellermann, L. C. Barbosa, O. L. Alves, *Phys. Rev. Lett.*, **89**, 235503 (2002).
26 R. D. Averitt, D. Sarkar, N. J. Halas, *Phys. Rev. Lett.*, **78**, 4217 (1997).

27 V. K. La Mer, R. H. Dinegar, *J. Am. Chem. Soc.*, **72**, 4847 (1950); V. K. La Mer, *Ind. Eng. Chem.*, **44**, 1270 (1952).
28 E. Matijevic, *Chem. Mater.*, **5**, 412 (1993).
29 M. A. Watzky, R. G. Finke, *J. Am. Chem. Soc.*, **119**, 10382 (1997) and references therein.
30 I. M. Lifshitz, V. V. Slyozov, *J. Phys. Chem. Solids*, **19**, 35 (1961).
31 C. Wagner, *Z. Elektrochem.*, **65**, 581 (1961).
32 T. Sugimoto, *Adv. Colloid Interface Sci.*, **28**, 165 (1987).
33 W. Ostwald, *Z. Phys. Chem.*, **37**, 385 (1901).
34 J. D. Livingston, *Trans. Metall. Soc. A. I. M. E.*, **215**, 566 (1959).
35 A. J. Ardell, R. B. Nicholson, *J. Phys. Chem. Solids*, **27**, 1793 (1966).
36 C. H. Kang, D. N. Yoon, *Metall. Trans. A*, **12**, 65 (1981).
37 C. K. L. Davies, P. Nash, R. N. Stevens, *J. Mater. Sci.*, **15**, 1521 (1980).
38 A. D. Brailsford, P. Wynblatt, *Acta Metall.*, **27**, 489 (1979).
39 P. W. Voorhees, M. E. Glicksman, *Acta Metall.*, **32**, 2001 (1984).
40 J. A. Marqusee, J. Ross, *J. Chem. Phys.*, **80**, 536 (1984).
41 M. Tokuyama, K. Kawasaki, *Physica A*, **123**, 386 (1984).
42 R. Viswanatha, C. Dasgupta, D. D. Sarma, unpublished results.
43 R. Viswanatha, P. K. Santra, C. Dasgupta, D. D. Sarma, to be published.
44 D. V. Talapin, A. L. Rogach, M. Haase, H. Weller, *J. Phys. Chem. B*, **105**, 12278 (2001).
45 E. M. Lifshitz, L. P. Pitaevskii, *Landau and Lifshitz Course of Theoretical Physics*, Vol. 10, Ch. 12, Butterworth-Heinemann, 1981.
46 G. Oskam, A. Nellore, R. L. Penn, P. C. Searson, *J. Phys. Chem. B*, **107**, 1734 (2003).
47 E. M. Wong, J. E. Bonevich, P. C. Searson, *J. Phys. Chem. B*, **102**, 7770 (1998).
48 E. M. Wong, P. G. Hoertz, C. J. Liang, B. Shi, G. J. Meyer, P. C. Searson, *Langmuir*, **17**, 8362 (2001).
49 N. S. Pesika, K. J. Stebe, P. C. Searson, *J. Phys. Chem. B.*, **107**, 10412 (2003).
50 N. S. Pesika, Z. Hu, K. J. Stebe and P. C. Searson, *J. Phys. Chem. B*, **106**, 6985 (2002).
51 Z. Hu, G. Oskam and P. C. Searson, *J. Colloid Interface Sci.*, **263**, 454 (2003).
52 G. Oskam, Z. Hu, R. L. Penn, N. Pesika, P. C. Searson, *Phys. Rev. E*, **66**, 11403 (2002).
53 R. Viswanatha, D. D. Sarma, *Chem. Eur. J.*, **12**, 180 (2006).
54 R. Viswanatha, S. R. Santra, S. Sapra, S. S. Datar, H. Amenitisch, D. D. Sarma, to be published.
55 Z. Hu, D. J. Escamilla Ramirez, B. E. Heredia Cervera, G. Oskam, P. C. Searson, *J. Phys. Chem. B*, **109**, 11209 (2005).
56 G. Beaucage, *J. Appl. Crystallogr.*, **28**, 717–728 (1995).
57 F. Buda, J. Kohanoff and M. Parrinello, *Phys. Rev. Lett.*, **69**, 1272 (1992).
58 M. V. Ramakrishna, R. A. Friesner, *Phys. Rev. Lett.*, **67**, 629 (1991).
59 (a) H. Fu, A. Zunger, *Phys. Rev. B.*, **55**, 1642 (1997); (b) H. Fu, A. Zunger, *Phys. Rev. B*, **56**, 1496 (1997).
60 P. E. Lippens, M. Lannoo, *Phys. Rev. B*, **39**, 10935 (1989).
61 J. M. Jancu, R. Scholz, F. Beltram, P. Bassani, *Phys. Rev. B*, **57**, 6493 (1998).
62 G. Allan, Y. M. Niquet, C. Delerue, *Appl. Phys. Lett.*, **77**, 639 (2000).
63 S. Sapra, N. Shanthi, D. D. Sarma, *Phys. Rev. B*, **66**, 205202 (2002).
64 S. Sapra, R. Viswanatha, D. D. Sarma, *J. Phys. D*, **36**, 1595 (2003).
65 S. Sapra, D. D. Sarma, *Phys. Rev. B*, **69**, 125304 (2004).
66 R. Viswanatha, S. Sapra, B. Satpati, P. V. Satyam, B. N. Dev, D. D. Sarma, *J. Mater. Chem.*, **14**, 661 (2004).
67 R. Viswanatha, S. Sapra, T. Saha-Dasgupta, D. D. Sarma, *Phys. Rev. B*, **72**, 045333 (2005).
68 L. Qu, W. W. Yu, X. Peng, *Nano Lett.*, **4**, 465 (2004).
69 L. B. Scaffardi, N. Pellegri, O de Sanctis, J. O. Tocho, *Nanotechnology*, **16**, 158 (2005).

70 G. Mie, *Ann. Phys.*, **25**, 377 (1908).

71 J. Turkevich, P. C. Stevenson, J. Hillier, *Discuss. Faraday Soc.*, **11**, 55 (1951).

72 R. Seshadri, G. N. Subbanna, V. Vijayakrishnan, G. U. Kulkarni, G. Ananthakrishna, C. N. R. Rao, *J. Phys. Chem.*, **99**, 5639 (1995).

73 R. Viswanatha, H. Amenitsch, D. D. Sarma, *J. Am. Chem. Soc.*, in press.

74 E. A. Meulenkamp, *J. Phys. Chem. B*, **102**, 5566 (1998).

75 R. Viswanatha, S. Sapra, S. Sen Gupta, B. Satpati, P. V. Satyam, B. N. Dev, D. D. Sarma, *J. Phys. Chem. B*, **108**, 6303 (2004).

76 (a) A. L. Efros, A. L. Efros, *Sov. Phys. Semicond.*, **16**, 772 (1982); (b) L. E. Brus, *J. Chem. Phys.*, **79**, 5566 (1983).

77 T. Vossmeyer et al., *J. Phys. Chem.*, **98**, 7665 (1994).

78 C. R. Bullen, P. Mulvaney, *Nano Lett.*, **4**, 2303 (2004).

79 W. W. Yu, L. Qu, W. Guo, X. Peng, *Chem. Mater.*, **15**, 2854 (2003).

80 L. Guo, S. Yang, C. Yang, P. Yu, J. Wang, W. Ge, G. K. L. Wong, *Chem. Mater.*, **12**, 2268 (2000).

81 J. Nanda, S. Sapra, D. D. Sarma, N. Chandrasekharan, G. Hodes, *Chem. Mater.*, **12**, 1018 (2000).